Electrical Power and Energy Systems 180 (2026) 112094

Contents lists available at ScienceDirect

International Journal of Electrical Power & Energy Systems

journal homepage: www.elsevier.com/locate/ijepes

Dynamic pricing optimization for load aggregators in virtual power plants considering user clustering and response behavior

Xiaolong Yang [a,*], Mengmeng Zhao [a], Weiyao Gao [a], Shuai Zhou [b], Jieping Han [a], Zeqi Ge [a], Yuhan Liu [a]

[a] School of Economics and Management, Northeast Electric Power University, Jilin 132012, China
[b] Department of Electrical and Electronic Engineering, Auckland University of Technology, Auckland 0620, New Zealand

ARTICLE INFO

Keywords:
Load aggregator
Virtual power plant (VPP)
Dynamic pricing
Stackelberg game
Renewable energy integration

ABSTRACT

Load aggregators (LAs) can integrate end users with adjustable loads within a specific region and participate in electricity spot markets to mitigate the growing peak–valley imbalance in power demand. As an important enabler of demand-side flexibility and user participation, LAs play a critical role in enhancing the operational efficiency of new-type power systems. This study proposes a two-stage dynamic pricing framework for LAs within virtual power plant (VPP) environments. In the first stage, a K-means++ clustering algorithm is applied to classify end users according to their load characteristics and demand response capabilities. In the second stage, a Stackelberg game is formulated to characterize the hierarchical interaction between the LA (leader) and end users (followers), taking into account operational constraints and market uncertainties. Four simulation scenarios are designed to validate the proposed model. The results show that the optimized pricing strategy reduces electricity costs by 3.57% for non-residential users and 2.45% for residential users, while improving load smoothness and LA profitability. The proposed framework provides a practical and scalable approach for optimizing LA pricing strategies and offers valuable insights for enhancing user participation and renewable energy integration in real-time electricity markets.

1. Introduction

With China's "dual-carbon" strategy deepening and the construction of a new-type power system accelerating, VPPs and LAs—as organizational forms that coordinate source-grid-load-storage and activate demand-side resources—are increasingly viewed as pivotal vehicles for achieving high renewable-energy penetration and advancing power-market reform [1,2]. While their functional emphases differ—VPPs focus on multi-energy complementarity and coordination across devices and stakeholders, whereas LAs emphasize aggregation of flexible user-side loads and market participation—their operating mechanisms are highly complementary. An emerging division of roles has taken shape in which VPPs orchestrate multi-energy control and LAs execute DR on the user side [3–5]. On the policy front, China's energy regulators have issued a series of instruments and technical guidelines to standardize VPP operations; among them, the Specification for VPP Operation and Management provides more actionable requirements on organizational boundaries, regulation-capacity assessment, market interfaces, and performance evaluation. According to that specification, by the end of 2023, 27 provincial-level regions had launched VPP pilots with aggregate callable regulation capacity exceeding 8000 MW, yet locally implemented commercial projects achieved an average return of only about 5.2%, markedly below the risk-adjusted return of conventional coal-fired assets [6]. Consequently, under a spot-oriented market with coupled day-ahead and real-time operations, designing pricing and incentive mechanisms for LAs that balance user responsiveness with aggregator profitability has become a key bottleneck to VPP commercialization [7,8]. Developing a paradigm for LA retail pricing and incentives that can operate amid volatility, incomplete information, and compliance constraints is therefore both practically urgent and methodologically valuable.

Research on LA operational decisions under the coupled day-ahead real-time mechanism largely falls into two camps. The first is cost-oriented optimization, which assuming attainable DR and stable price elasticity—uses robust models to determine retail prices or power schedules [9,10]. Even when wind-solar-thermal-storage portfolios are included and "two-stage" or "day/intraday" formulations are adopted

* Corresponding author.
E-mail addresses: yangxiaolong@neepu.edu.cn (X. Yang), 15144257125@163.com (M. Zhao), gaoshangkuaile1001@163.com (W. Gao), zoey.zhou@aut.ac.nz (S. Zhou), 20100414@neepu.edu.cn (J. Han), gzq1472580369@163.com (Z. Ge), 13324425328@163.com (Y. Liu).

https://doi.org/10.1016/j.ijepes.2026.112094
Received 25 November 2025; Received in revised form 14 July 2026; Accepted 29 July 2026
Available online 31 July 2026

Nomenclature

LA	Load Aggregator
EG	External Grid
DR	Demand Response
PSVF	Peak-shaving and Valley-filling
VPP	Virtual Power Plant
$L'_{c,t}$	Outlier-corrected value
f_1,e_1	Step size before/after in outlier processing
$L_{r,t}$	Normalized load of the k-th sample at time
$L_{q,t}$	Load series over all time points
Y_a	Compensation paid by EG for purchasing PSVF services
P_g	LA real-time purchasing power
V_{cf}	LA power procurement cost
p_{bc}^{ny}	Per-kWh compensation from EG to LA for PSVF participation
P_{fg}	LA real-time power during PSVF
W_z	LA net profit
E_{ls}	LA retail sales revenue
Y_b	Incentive payment from LA to end users for PSVF participation
p_{ls}	LA retail tariff
P_s	LA real-time retailing power
G_{fh}	LA administrative cost
p_{bc}^{fh}	Per-kWh compensation from LA to end users for PSVF
P_{xy}	End-user contributed load during DR
P_l	Losses when supplying power from EG to LA
$P_{s,\min}$	Minimum retail power
$P_{s,\max}$	Maximum retail power
H_{yh}	Net benefit of end-user electricity use
D_{yh}	End-user utility of electricity use
J_z	Planned consumption of an end user over a period
J_{jc}	End-user-adjustable-load responsiveness
α	End-User Variable Load Response
J_{kb}^{pj}	Historical average of end-user adjustable load
a,b	Utility coefficient reflecting the nonlinearly increasing utility of electricity use
$J_{\min}$	Essential-electricity consumption of end users
$J_{\max}$	Maximum electrical capacity of equipment
z	Inter-period load change limit
P_{jc}	Real-time base-load power
P_1	Real-time residential load power
P_2	Real-time flexible-load power
P_{all}	Aggregate load of all registered end users in the VPP campus eligible for LA DR

[11,12], limited characterization of market feedback and user heterogeneity constrains the closed-loop price-response elasticity. The second camp is data-driven policy learning: for example, deep reinforcement learning can learn dynamic pricing under weak mechanistic assumptions [13–15], but it suffers from limited interpretability and maintainability, and it demands substantial computing resources, online exploration, and strict safety margins—hindering engineering deployment. More critically, engineering realities are often underemphasized: users' price sensitivity is markedly time-varying, nonlinear, and subject to threshold effects [16]; meanwhile, real-time deviations and ancillary-service assessments impose default penalties or opportunity costs that enlarge the LA's risk exposure and profit variance [17,18], distorting model outputs. Additionally, in the peer-to-peer (P2P) trading scenario of multi-integrated energy systems (IES), some studies have constructed a distributed optimization framework based on asymmetric Nash negotiation and combined it with an improved ADMM to achieve privacy-preserving joint quantity-price decision-making, which can provide a methodological reference for the pricing-game modeling in this paper [19–21]. To narrow this gap, recent work has employed Stackelberg games to explicitly capture the price-quantity interaction between LAs and commercial-industrial users [22,23], and has proposed methods for identifying and quantifying adjustable loads in the retail sector to improve parameterization and attainability assessments [24,25]. In summary, two shortcomings persist: (i) uniform pricing based on an "average user" with insufficient segmentation and targeted incentives by DR capability; and (ii) inadequate endogenization of time-varying price elasticity and compliance costs such as default penalties, leading to a disconnect between strategy and actual operation.

Building on the above, this paper proposes a real-time pricing strategy for LAs within the VPP context, formulated as a leader–follower (Stackelberg) game. First, we construct a coordinated supply mechanism between the external grid and the LA under the VPP framework, and classify end users via clustering according to their consumption characteristics and DR capability. Second, we develop optimization-based pricing models for the LA side and the end-user side, analyze their strategic interaction in pricing decisions, and establish a Stackelberg game with the LA as leader and end users as followers. Compared with existing studies, the contributions of this study are as follows:

(1) We propose a two-stage "clustering-game pricing" framework that couples K-means++ clustering—based on end-user consumption characteristics with a Stackelberg leader–follower game, thereby co-optimizing LA pricing and user response.
(2) We incorporate incentive constraints and a default-penalty mechanism into the payoff function to strengthen the model's risk-control capability under market volatility and user uncertainty.
(3) Through multi-scenario simulations, we validate the model's effectiveness: the strategy simultaneously increases LA profits and reduces users' electricity costs, while improving the smoothness of the load profile.

The remainder of this paper is arranged as follows: In Section 2 presents the problem definition and system architecture, detailing the interactions among the VPP, LA, and end users. In Section 3, develops a capability-aware user modeling and stratification approach—including feature selection, clustering implementation, and the estimation of price elasticity and baselines—and formulates an LA dynamic pricing Stackelberg model for the coupled day-ahead-real-time setting. In Section 4, describes the solution strategy: a coordinated procedure combining an outer genetic algorithm with an inner CPLEX-based user-response solver, along with feasibility-repair steps and convergence criteria. In Section 5, reports case studies and experimental results, covering park-level data, scenario configuration, baseline comparisons, and sensitivity analyses. The last section outlines our discussion and conclusions.

2. VPP-based LA architecture and trading mechanisms

2.1. Physical structure and market framework

The interaction framework of the LA under the VPP context is shown in Fig. 1 From the physical perspective, the system comprises three parts: (1) a VPP management layer, including composite control systems, distributed generation units, and energy storage devices; (2) an LA control layer, consisting of smart meters, edge-computing terminals, and communication-control equipment for real-time monitoring and load

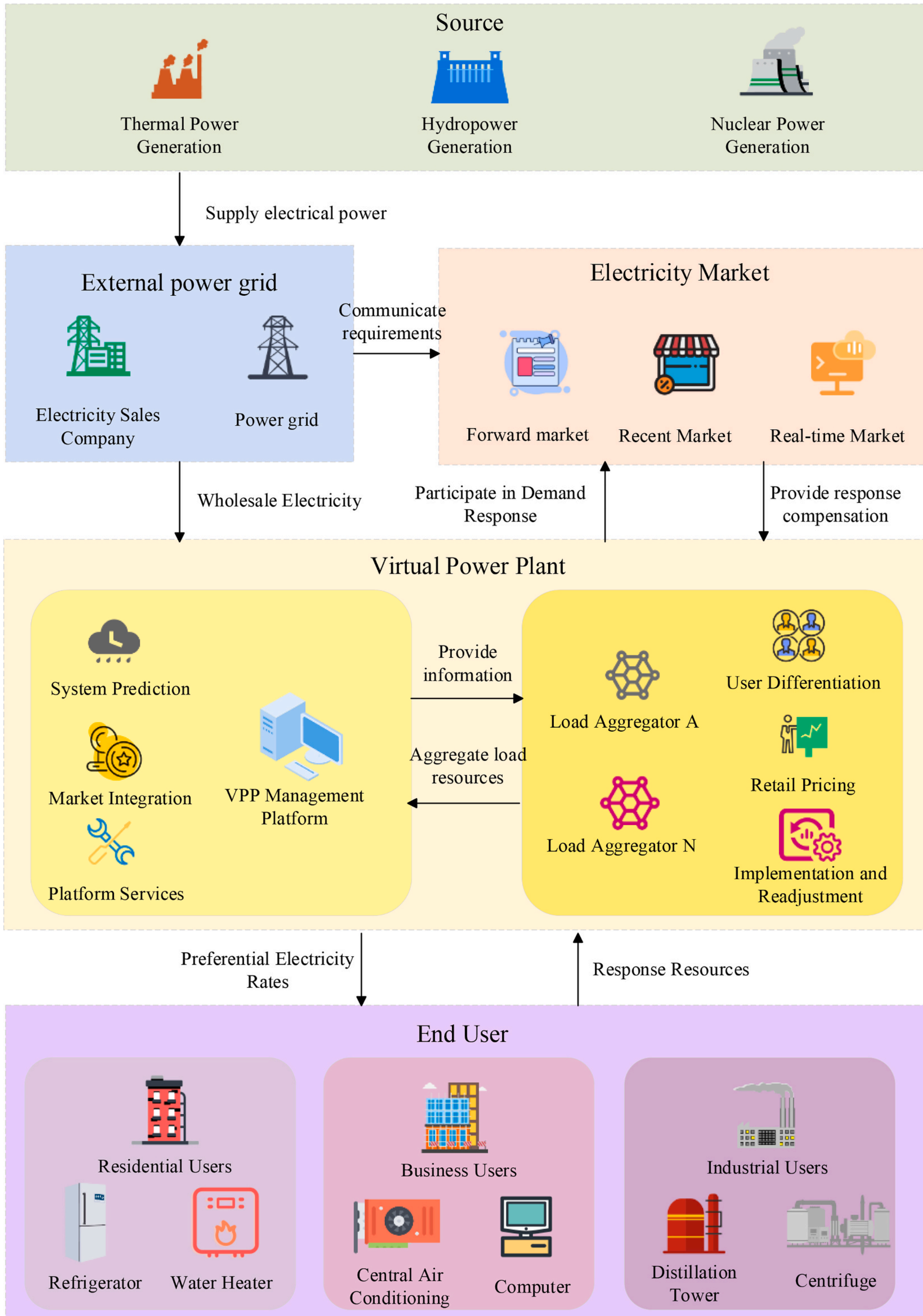

Fig. 1. System framework for LA participation in DR and electricity markets under a VPP platform.

dispatch; and (3) an end-user layer that covers multiple user categories, such as industrial, commercial, and residential customers [26,27].

In the VPP setting, electricity trading within an industrial park involves three basic economic entities: the electricity supplier, the park-level LA, and end users. High-speed, reliable, bidirectional information exchange among the three enables real-time transmission of price signals and DR information. The external grid, as the wholesale supplier, determines the baseline electricity price [28,29]. Guided by market signals and user characteristics, the LA sets retail tariffs and offers incentive prices to attract end users to sign contracts and participate in DR [30]. Based on load characteristics, end-user loads in the park can be clustered into four categories: routine residential loads; semi-flexible loads (interruptible but non-shiftable, and shiftable but non-interruptible); flexible loads; and non-interruptible loads. By recruiting DR-capable portions of the first three categories to engage in peak-shaving and valley filling, the LA earns price-spread revenues, and can

Table 1
Clustering algorithm comparison at K = 4.

Method	Silhouette	DBI	CH
K-means++	0.3675	1.0510	1368.49
GMM	0.3630	1.0678	1349.46
Hierarchical (Ward)	0.3571	1.0547	1320.69

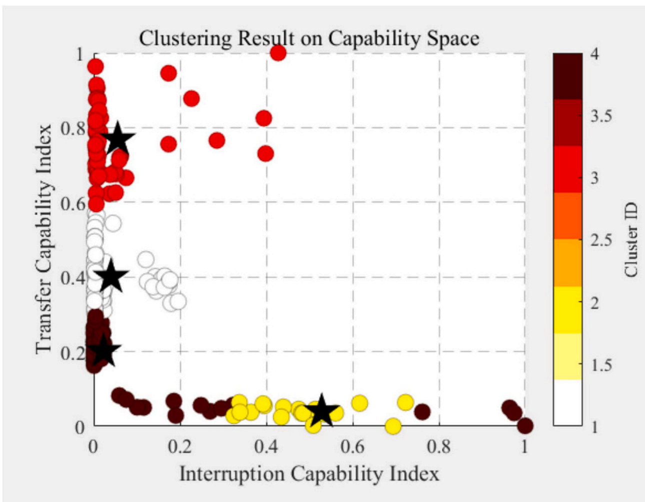

Fig. 2. Results of the Clustering Analysis.

further obtain compensation by aggregating loads to provide intraday peak regulation [31–33]. In this architecture, the VPP acts as the overall operator of the park—coordinating wind turbines, energy-storage systems, and energy-coupling devices, and overseeing energy transactions and control among the electricity supplier, the LA, and other purchasing agents—to ensure supply–demand balance and economic operation at the park level [34–36].

2.2. Market trading mechanisms and strategies

In the proposed model, the LA and end users are independent economic agents. The LA maximizes its net profit by monitoring the operating states of its assets and setting dynamic buy-sell electricity prices. End users, guided by the LA's price signals, optimize their consumption strategies and the extent of their DR participation to maximize the difference between consumption utility and electricity cost. Accordingly, LA pricing decisions must account for both the aggregator's own profit and user responses, forming a typical strategic interaction between the two sides.

On this basis, the interaction between the LA and end users is modeled as a Stackelberg game. The LA, as the upper-level decision maker (leader), holds priority in setting prices; end users, as lower-level decision makers (followers), adjust their load strategies according to the LA's price signals and feed back their responses. The proposed leader–follower model targets day-ahead optimal scheduling and characterizes the LA's dynamic pricing mechanism and multi-actor response behavior within the VPP framework.

3. Clustering analysis and construction of a Stackelberg-based bidding model

3.1. K-means++ based clustering analysis of end-use energy devices

We justify the use of K-means++ by comparing it with representative alternatives (e.g., GMM and hierarchical clustering/DBSCAN) under the same feature set with K = 4. Standard validity indices (silhouette, DBI, CH) and runtime are reported in Table 1 K-means++ achieves competitive compactness/separation with low computational cost and clear engineering interpretability; thus, it is adopted for Stage-1 user clustering.

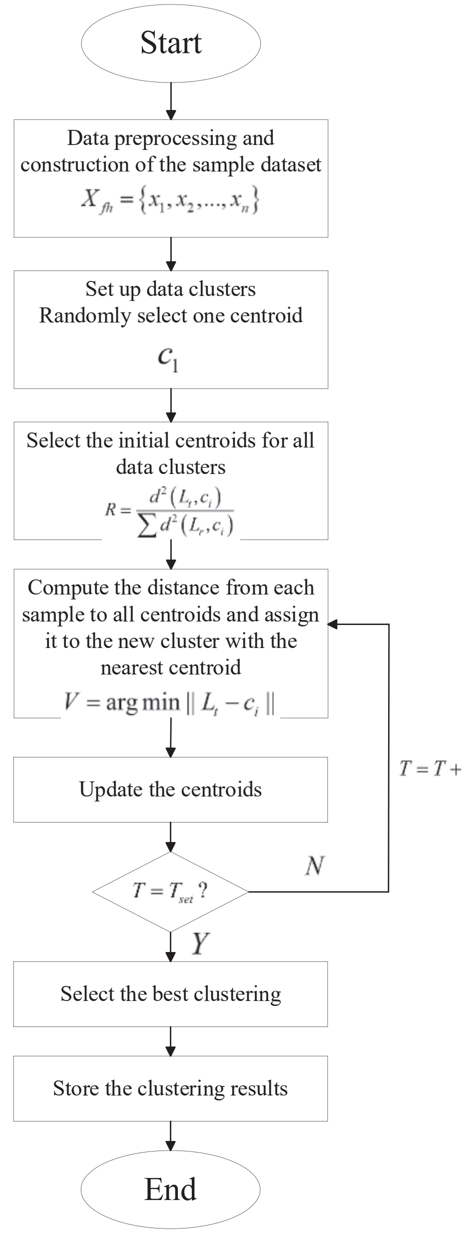

Fig. 3. Data cleansing workflow.

To characterize the schedule ability of end-use devices, this study constructs a dataset with four key feature dimensions—maximum interruption duration, interruption response delay, maximum ratio of transferable power, and post-transfer sustaining time [37–40]. During data generation, multiple sample sets are created on the MATLAB platform for three representative user categories (residential, commercial-industrial, and industrial), and Monte Carlo simulation is employed to ensure randomness and reasonable distributions. Aggregating the typical daily load curves of these user types yields an initial set of load profiles,$X_{fh} = \{x_1, x_2, \ldots, x_n\}$ where each profile x_i contains s sampling points. Given a commonly used sampling interval of 15 min,$s = 96$. A clustering algorithm is then applied to identify the load-response characteristics of different end-user groups, with the clustering results visualized in Fig. 2. This lays a data foundation for user segmentation

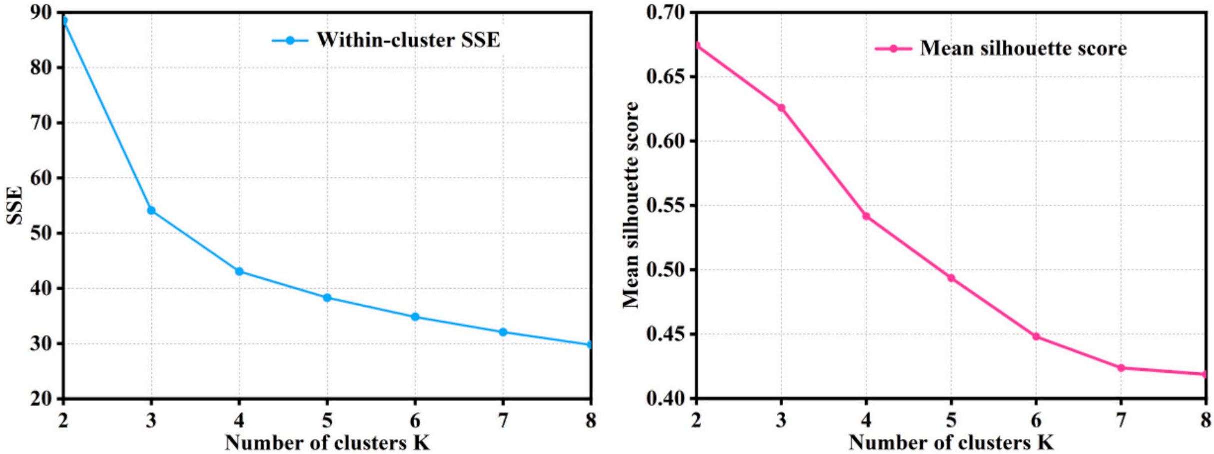

Fig. 4. Determination of the number of clusters K using SSE (elbow) and silhouette analysis.

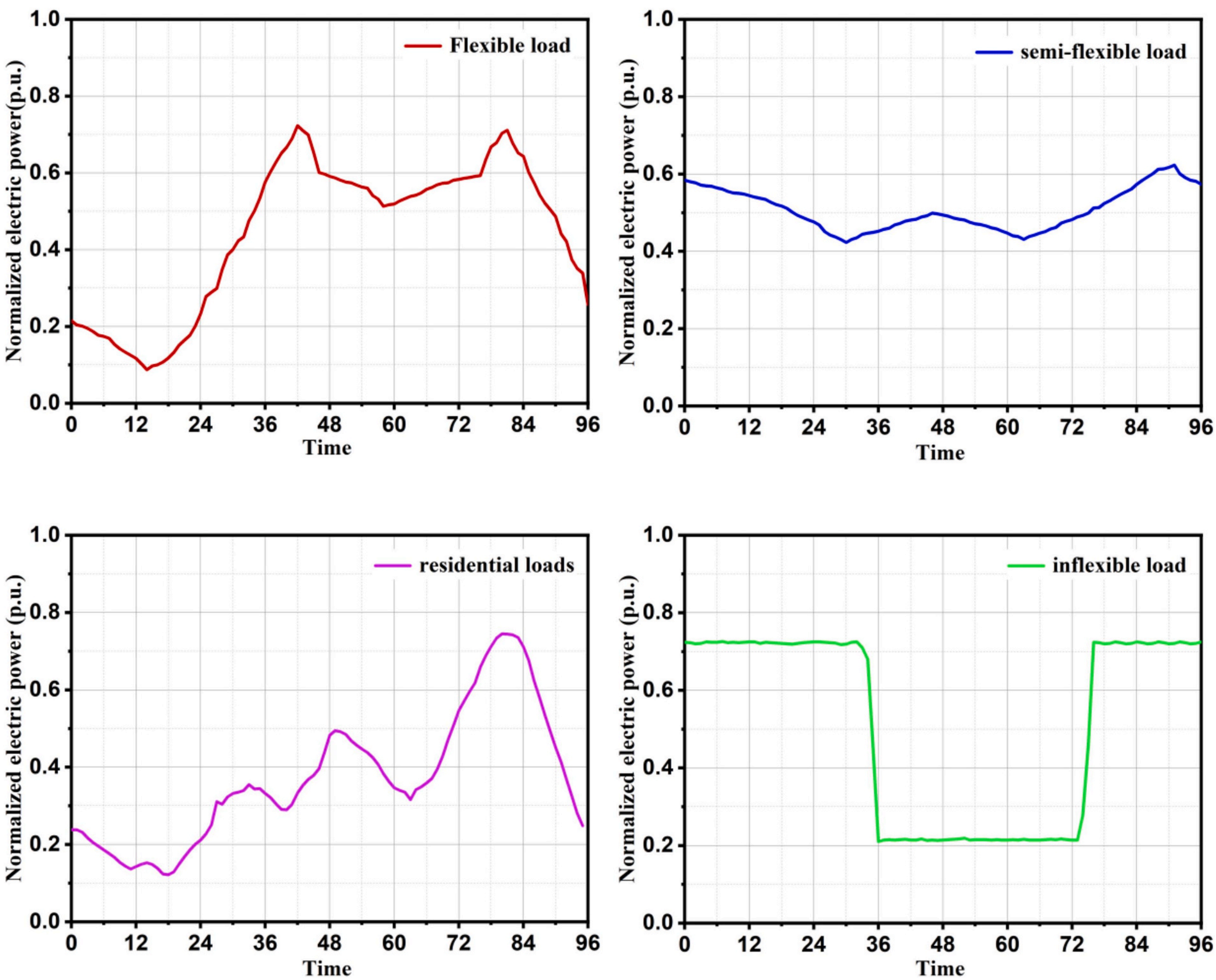

Fig. 5. Energy-use load curves by cluster for end users after the clustering analysis.

and parameter setting in the subsequent LA pricing and game-theoretic modeling.

During data cleansing, following [41,42], each load curve in the set x_i is examined to detect anomalies such as missing entries, abrupt jumps, and negative values. If the share of missing/anomalous data on a curve exceeds a preset threshold, that curve is deemed invalid and removed. Let Q denote the number of valid samples after removal. For the $q-th$ load curve, if the measurement at time t_c(denoted $L_{c,t}$) is anomalous, it is corrected using a smoothing formula, as follows:

$$L'_{c,t} = \frac{\left(\sum_{f=1}^{f_1} L_{c,t-f} + \sum_{e=1}^{e_1} L_{c,t+e}\right)}{(f_1 + e_1)} \tag{1}$$

where f and e index the backward and forward-looking sampling points, respectively,f_1 and e_1 are the corresponding window lengths; they are set according to practical needs and are typically taken as 5.

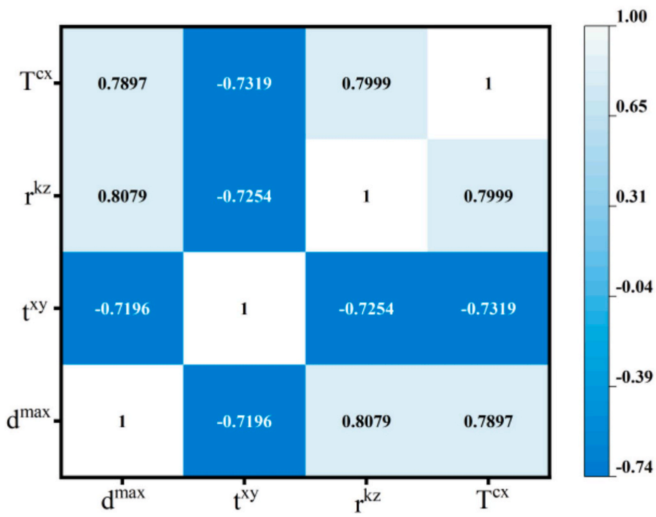

Fig. 6. Spearman correlation (normalized features) heatmap.

Next, a max–min normalization is applied to the load data so that terminal devices with different magnitudes but belonging to the same user category are comparable, thereby eliminating dimensional effects and improving reliability. The normalized value is given as follows:

$$L_{r,t} = \frac{L_{r,t} - \min L_{q,t}}{\max L_{q,t} - \min L_{q,t}} \tag{2}$$

Where max $L_{q,t}$ and min $L_{q,t}$ denote the maximum and minimum load values over all time points on the curve, and $L_{r,t}$ denotes the normalized load of the $r-th$ sample at time t Consequently, the normalized sample values lie within [0–1]. After preprocessing, the daily load-curve dataset is obtained as $X_{cl} = \{x'_1, x'_2, \ldots, x'_n\}$. The detailed implementation steps of data cleansing and preprocessing are illustrated in Fig. 3.

To determine the number of clusters, we evaluate K = 2–8 using the elbow method and the mean silhouette score. As shown in Fig. 4, the within-cluster sum of squares (SSE) decreases rapidly when K increases from 2 to 4, while the marginal improvement becomes limited for K > 4, indicating an elbow around K = 4. Fig. 4 reports the mean silhouette score, which reflects both within-cluster cohesion and between-cluster separation. Although the silhouette score decreases with larger K, K = 4 provides an acceptable trade-off between compactness, separation, and engineering interpretability. Therefore, we set K = 4 for subsequent user clustering.

After clustering, the original end users are regrouped into four clusters, as shown in Fig. 5 The reclassification rate reaches 76.7%, effectively breaking the prior categories of industrial, commercial-industrial, and residential users. The third and fourth clusters are excluded from subsequent analysis: the third is dominated by residential loads that cannot effectively participate in DR (e.g., lighting and small household appliances), while the fourth consists of loads that typically run for long durations and are generally non-interruptible, such as municipal administrative loads, industrial reactors and distillation columns, and residential refrigerators.

3.2. Feature relevance and redundancy analysis

To justify the selected clustering attributes and examine potential redundancy among them, we conduct a feature relevance and multicollinearity analysis on the normalized feature set. For clarity, the four clustering features are denoted as:d^{max}(maximum interruption duration),t^{xy}(response delay),r^{kz}(transferable power ratio), and T^{cx}(duration after load transfer). These attributes characterize demand response capability from complementary aspects, i.e., interruptibility, response speed, adjustable capacity, and sustainability after shifting.

Table 2
Variance Inflation Factor (VIF) of selected features.

Feature	VIF	Interpretation
d^{max}	3.61	VIF < 5 (no severe multicollinearity)
t^{xy}	2.62	
r^{kz}	3.66	
T^{cx}	3.29	

Fig. 6 reports the Spearman correlation matrix of the normalized features. Spearman correlation evaluates monotonic relationships based on rank information and is thus more robust to non-Gaussian distributions and outliers than purely linear correlation measures. The results indicate that t^{xy} is negatively correlated with the flexibility-related attributes(d^{max},r^{kz}, and T^{cx}), which is consistent with the physical intuition that faster-responding users tend to have stronger flexibility and larger adjustable capacities. Meanwhile d^{max},r^{kz}, and T^{cx} exhibit positive correlations, reflecting that users with higher interruptibility often also have higher transferable ratios and longer post-transfer sustainability. Importantly, although several feature pairs are correlated as expected, the overall correlations do not suggest that the attributes are duplicates of each other; instead, they provide complementary information for distinguishing heterogeneous demand response capabilities in the user population.

To further quantify redundancy, Table 2 reports the variance inflation factor (VIF) of each feature. VIF measures how much the variance of a regression coefficient is inflated due to multicollinearity with the other predictors, and values below 5 are commonly regarded as indicating no severe multicollinearity. As shown in Table 2, all features have VIF values below 5, demonstrating that the selected attributes do not suffer from severe multicollinearity and thus remain informative for clustering.

3.3. Construction of a bidding model based on a Stackelberg game

At the upper level, the leader is the LA, whose operating objective is to maximize net profit. The objective is affected by (i) revenue from retail energy sales to end users within the VPP park, (ii) the cost of purchasing electricity from the external grid and the associated management cost, and (iii) incentive payments made to end users for participating in DR. The objective function is given as follows:

$$\max W_z = \sum_{t=1}^{T} [E_{ls} - Y_b] + Y_a - G_{fh} - V_{cf} \tag{3}$$

$$E_{ls} = p_{ls} P_s \Delta t \tag{4}$$

$$Y_a = \sum_{t=1}^{T} \left(p_{bc}^{ny} |P_{fg}| \Delta t\right) \tag{5}$$

$$Y_b = p_{bc}^{fh} |P_{xy}| \Delta t \tag{6}$$

where W_z is the LA's net profit;E_{ls} is the retail revenue from selling electricity to end users;Y_a is the compensation paid by the EG to the LA for providing peak-shaving and valley-filling (PSVF) services;Y_b is the incentive expenditure the LA pays to end users for participating in PSVF;V_{cf} is the LA's electricity-purchase cost; and G_{fh} is the LA's annual management/overhead cost.p_{ls} denotes the retail electricity price charged by the LA;p_{bc}^{ny} is the per-kWh compensation rate paid by the EG to the LA for PSVF;P_{fg} is the real-time power provided by the LA for PSVF (its absolute value is used in calculation).P_s is the LA's real-time retail power supplied to end users;p_{bc}^{fh} is the per-kWh incentive rate the LA pays to end users for PSVF participation; and P_{xy} is the load contribution of end users when responding—positive for reductions in consumption and negative otherwise.

At the lower level, the followers are end users with controllable loads. End users who procure electricity via the LA aim to maximize their consumption utility, with the relevant factors being their electricity consumption across user categories. The objective function is described as follows:

$$\max H_{yh} = D_{yh} - p_{ls}J_z \tag{7}$$

$$D_{yh} = aJ_z - bJ_z^2 \tag{8}$$

$$J_z = J_{jc} + \alpha J_{kb}^{pj} \tag{9}$$

$$J_{jc} = \sum_{t=1}^{T} \left(P_{jc}\Delta t\right) \tag{10}$$

$$\alpha = \frac{\sum_{t=1}^{T}(P_1\Delta t + P_2\Delta t)}{P_{all}} \tag{11}$$

where H_{yh} denotes the difference between the end user's electricity-use utility and electricity cost;D_{yh} is the user's satisfaction with electricity use, assumed to be non-decreasing and concave and modeled by a quadratic form in this paper;J_z is the total planned electricity consumption of the end user within a cycle. Parameters a and b are utility coefficients that capture the nonlinear (concave) increase of electricity-use utility.P_{jc} is the baseline power;J_{jc} is the baseline load of the end user;α is the response ratio of the user's adjustable load;J_{kb}^{pj} is the historical average of the user's adjustable load.P_1 and P_2 denote the load power of different user categories, and P_{all} is the total load power of all end users registered within the VPP park that can participate in the LA's DR services.

3.4. Constraints

3.4.1. LA's selling-power constraint

When the LA buys and sells electricity, unavoidable transmission losses occur. Denote the loss by P_l.The delivered (retail) power as follows:

$$P_s = P_g - P_l \tag{11}$$

Moreover, due to the "produce-and-consume instantly" property of electricity, the selling power is bounded by end-user demand. Using the historical daily extrema within the LA's service area, we impose:

$$P_{s,\min} \leqslant P_s \leqslant P_{s,\max} \tag{12}$$

3.4.2. Purchase-cost constraint

An end user's purchase cost (retail price)p_{ls} should not exceed the real-time external-grid price at the time of purchase. This can be expressed as:

$$V_{cf} \geqslant p_{ls} \tag{13}$$

where V_{cf} denotes the LA's electricity purchase cost from the external grid. This constraint ensures that the end user's expenditure will not exceed the EG's real-time selling price, guaranteeing rational choice.

3.4.3. Demand-response constraint

The LA affects user demand by adjusting prices or incentive schemes. This constraint ensures that the LA's selling power P_s does not exceed the upper bound of the actually available responsive capacity, as follows:

$$P_s^{ky} \geqslant P_s \tag{14}$$

where P_s^{ky} denotes the upper limit of available response resources; the LA can sell only up to its maximum deliverable power so as not to exceed the usable capacity.

Table 3
Mapping from clusters to response-capability parameters in the game model.

Cluster k	Type (from clustering)	Robustness to initialization
1	Flexible	0.35
2	Semi-flexible	0.22
3	Residential-dominated	0.12
4	Inflexible	0.05

3.4.4. End-user load power and ramping constraints

We also impose constraints on energy use and on the smoothness of power changes:

$$J_{\min} \leqslant J_z \leqslant J_{\max} \tag{15}$$

$$|P_{jc}^{t} - P_{jc}^{t-1}| \leqslant z \tag{16}$$

where $J_{\min}$ is the user's minimum required energy,$J_{\max}$ is the maximum usable energy of the end-user equipment, and z is the bound on period-to-period power variation.

3.4.5. Response-capability constraint.

Since the LA allocates power according to users' demand-response capability, the response ratio must not exceed an upper bound:

$$\alpha \leqslant \alpha_{k(j)}^{\max} \tag{17}$$

where $\alpha_{k(j)}^{\max}$ is the maximum achievable response capability of user j, determined by its cluster $k(j)$ from Stage 1.

3.4.6. Power-supply constraint

The power supply is limited by the capacity of end-user loads within the park that participate via the LA; that is, the aggregate load of all end users must not exceed the total supply capability, as follows:

$$\sum_{i=1}^{N} P_i \leqslant P_{all} \tag{18}$$

where P_{all} denotes the total load of end users in the park that participate via the LA.

4. Solution methodology

4.1. Solving the Stackelberg game

Stage-1 clustering results are embedded into the Stackelberg game by assigning cluster-dependent response limits. After clustering, end-users are grouped into four clusters, and each j cluster is associated with a maximum response capability $\alpha_{k(j)}^{\max}$. The mapping relationship between user clusters and response capability parameters is presented in Table 3. In the follower model, the response ratio of users in cluster j is bounded by $\alpha_{k(j)}^{\max}$, which yields differentiated response capabilities across clusters.

As the leader in the game, the LA—after obtaining the DR-capable end-user load power and the day's load profiles from the clustering analysis—aims to maximize its profit. As followers, end users aim to maximize the difference between their electricity-use utility and electricity cost, and they adjust their time-of-use strategies in response to the LA's retail prices and real-time load factors. Accordingly, the bidding process by which the LA participates in the spot market can be modeled as a Stackelberg game, which can be expressed as follows:

$$S = \{L, U, F\} \tag{19}$$

The game model comprises the three basic elements of a Stackelberg game: the set of players L, strategy set U and payoff function F. In the gaming process, the LA uses the retail price p_{ls} as its strategy set U_s to adjust its profit W_z; end users adopt the time-varying responsive-load ratio α as their strategy set U_x to adjust the difference between electricity-use utility and cost H_{yh}. During the game, the followers optimally respond to the leader's strategy, and the leader accepts the returned response; the outcome at which the game reaches equilibrium is the Stackelberg equilibrium. In this paper, the Stackelberg equilibrium $\left(U_s^*, U_x^*\right)$ satisfies:

$$\begin{cases} W_z\left(U_s^*, U_x^*\right) \leqslant W_z\left(U_s, U_x^*\right) \\ H_{yh}\left(U_s^*, U_x^*\right) \leqslant H_{yh}\left(U_s^*, U_x\right) \end{cases} \tag{20}$$

Given the follower's best response U_x^*,the leader cannot improve its payoff by unilaterally changing U_s;and given the leader's strategy U_s^*,the follower cannot improve its payoff by unilaterally changing U_x. When all players adopt their Stackelberg equilibrium strategies, no party can improve its payoff through unilateral deviation.

Assume the follower utility is continuous and strictly concave in the follower decision variables, and the follower feasible set is nonempty, convex, and compact. Moreover, assume the leader decision variables are bounded by (12)–(14). Then, for any feasible leader decision, the follower problem admits a unique optimal response. Furthermore, the leader problem attains an optimum; hence, a Stackelberg equilibrium exists.

4.2. Solution procedure

The proposed LA pricing model is a nonlinear bilevel game-theoretic optimization problem. Nonlinearity mainly arises from the interaction between the LA's profit-maximization objective in the upper-level game and the end users' utility-maximization objective in the lower level. We first initialize a set of admissible pricing strategies for the LA, which serve as predicted retail prices for each time period. Based on historical data and market analysis, Monte Carlo simulation combined with scenario reduction is used to emulate price volatility under different conditions, capture the evolution of related factors, and forecast end users' DR participation. The LA's retail-pricing strategy is then adjusted through the game in response to feedback on DR intensity. In each iteration, the LA updates prices according to user responses with the goal of maximizing profit. In the lower-level model, DR is determined by the end users' utility-maximization problem, and the maximization of consumer surplus becomes a key principle for setting prices.

In the solution process, the upper-level pricing problem is solved using a genetic algorithm, which iteratively searches for the optimal pricing strategy and yields the LA's retail prices. The lower-level demand-response decisions are obtained by solving the end users' utility-maximization problem [43,44], for which an exact optimization solver (e.g., CPLEX) is employed to compute the optimum.

The genetic algorithm (GA) is a population-based metaheuristic inspired by biological evolution. By simulating iterative genetic processes, it gradually approaches the optimum and is well suited to complex, high-dimensional, and nonlinear optimization problems, enabling effective search over large solution spaces. In this study, the lower-level optimization outcomes—i.e., end-user response levels—serve as conditions for the upper-level model and are iterated to convergence toward the optimal solution. Given the problem's complexity, the GA is an effective choice because it does not require derivatives of the objective function; instead, it optimizes by evaluating and selecting candidate solutions.

CPLEX is an optimization package capable of solving complex linear and quadratic programming problems. It searches for the optimum within the feasible region with high efficiency and accuracy, making it suitable for large-scale, high-precision applications. By leveraging multicore processors and distributed computing, CPLEX enables parallel computation: decomposing a problem into multiple subproblems and solving them concurrently can substantially accelerate the solution process.

The proposed pricing–response problem exhibits a coupled bilevel structure with non-smooth terms and multiple operational constraints,

Table 4
Qualitative comparison of candidate solvers for the proposed bilevel pricing problem.

Method	Handles non-smooth/ constraints	Robustness to initialization	Typical convergence
GA	Strong	High	Moderate
PSO	Medium	Medium	Fast but may stagnate
DE	Medium–strong	Medium–high	Moderate

which makes gradient-based deterministic solvers less robust. To justify the choice of GA as the outer-layer search, Table 4 provides a qualitative comparison between GA and common metaheuristics (PSO and DE).

As summarized in Table 4, GA offers strong robustness for non-smooth constrained problems and is straightforward to integrate with the inner-layer solver. Therefore, the "outer GA + inner exact solver (e.g., CPLEX)" framework is adopted, as illustrated in Fig. 7.

5. Case study

5.1. Data description

Taking Park A of a Shandong VPP pilot project as an example: the park contains 20 industrial enterprises (e.g., prepared-food processing, packaging manufacturing, and electronics assembly). Based on metering by the VPP park management platform and the peak averages on working days in March—May 2024, the typical daily peak load is about 50 MW. There are 43 commercial-industrial enterprises (including 40 restaurants and three seven-story office buildings with a 60% utilization rate); combining contracted grid-connection capacities with building energy-use densities yields a typical daily peak load of about 20 MW. For 5,800 residential users, using smart-meter data and an estimate based on "per-household capacity × coincidence factor" the typical daily peak load is about 30 MW. The park's total peak load is therefore ~100 MW. The shares by load category align with the time-of-use proportions recorded by the VPP management platform during the same period and satisfy the criteria for classifying the site as a "balanced-type park" The load shares within the park are shown in Tables 5 and 6. Among them, data for industrial users and some commercial-industrial users are from field measurements; gaps in energy-use data for residential users and for certain restaurants and office buildings are filled by short-term forecasting.

The LA's purchase price is set with reference to the latest tariff standards at the location of Park A, using the March (spring) tariff level for calculation. For non-residential users, differentiated pricing is applied across five daily periods—deep off-peak, off-peak, flat, peak, and super-peak—whereas the residential tariff is uniformly computed using the lowest tier of the block tariff (0.555 CNY/kWh). The park is connected at a voltage level of 10 kV, so non-residential users are subject to the highest tariff tier; the specific rates are listed in Table 7. The LA offers contract incentives to end users in the form of retail-price discounts. Because some commercial-industrial and industrial users had already reduced costs through load shifting before contracting with the LA, the incentive is implemented via load-factor incentive bands: when a user's load factor falls within the designated band, a consumption-compensation mechanism is triggered.

In addition to the margin from organizing controllable loads to provide peak-shaving and valley filling (i.e., the difference between compensation from the external grid and incentives paid to users), the LA also receives compensation from the external grid when demand-response events are triggered, which depends on the system load factor ρ and its deviation from the security threshold. For this part, we adopt a piecewise (optionally nonlinear) compensation scheme as follows:

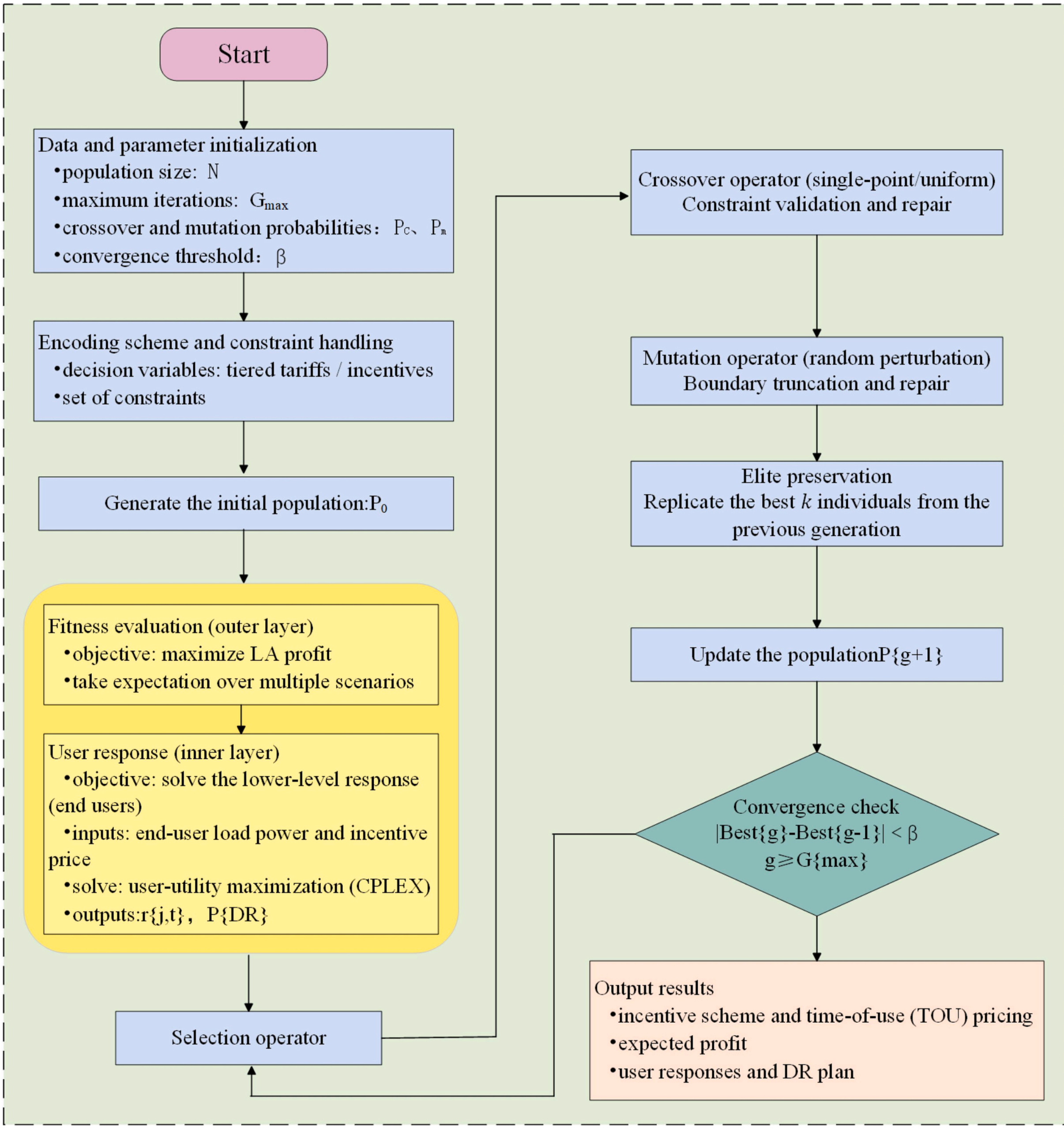

Fig. 7. Model solution procedure.

Table 5
Data sources and key simulation settings for the Shandong park case.

Item	Source	Resolution/value
Industrial & commercial loads	Park metering system	15-min
Residential aggregated load	Smart meter aggregation	15-min
Tariff (TOU)	Utility published tariff	time-of-use periods
DR events & controllability logs	DRMS platform	event logs
Time step	DRMS platform	15-min
Distribution loss rate	/	3%
GA population/generations	/	50/100
Crossover/mutation	/	0.8/0.05

(1) When $\rho \geqslant \rho_J$(peak period), peak-shaving compensation applies: the base rate is 0.30 CNY/kWh, increasing linearly with ρ at a slope of 3.0 CNY/kWh per unit load factor, capped at 0.60 CNY/kWh at$\rho = 1$.

Table 6
Energy-use distribution of end users in the VPP Park A.

End-User Category	Load Share	Load (MW)	Coincidence Factor
Industrial Users	50%	50	0.88
Commercial Users	20%	20	0.92
Residential Users	30%	30	0.55

(2) When $\rho \leqslant \rho_S$(deep off-peak with surplus), valley-filling compensation applies: the base rate is 0.10 CNY/kWh, increasing with a slope of 1.50 CNY/kWh per unit load factor, capped at 0.25 CNY/kWh.

In addition, the LA pays an annual management fee to the VPP park and covers operating expenses such as staff salaries and maintenance/inspection of related equipment, totaling 1.4 million CNY per year. Line

Table 7
March time-of-use (TOU) electricity prices for a given city.

Period type	Time span	Price (CNY/kWh)
Deep Off-Peak	11:00–14:00	0.23
Off-Peak	10:00–11:00 14:00–17:00	0.332
Flat	22:00–10:00	0.689
Peak	20:00–22:00	1.04
Super-Peak	17:00–20:00	1.2

Table 8
Other basic parameters.

Description	Parameter	Value
Annual management cost of the LA	G_{fh}	1.4 million CNY/year
Upper threshold of load factor for triggering EG compensation	ρ_J	0.9
Lower threshold of load factor for triggering EG compensation	ρ_S	0.55
Compensation base from EG during peak-shaving	C_{xf}	0.3 CNY/kWh
Maximum compensation from EG during peak-shaving	$C_{xf}^{\max}$	0.6 CNY/kWh
Compensation base from EG during valley filling	C_{tg}	0.1 CNY/kWh
Maximum compensation from EG during valley filling	$C_{tg}^{\max}$	0.25 CNY/kWh
Incremental slope of EG compensation during peak shaving	θ_{xf}	3 CNY/kWh
Incremental slope of EG compensation during valley filling	θ_{tg}	1.5 CNY/kWh
Upper load-factor threshold for triggering LA incentives	η_J	0.95
Lower load-factor threshold for triggering LA incentives	η_S	0.65
LA per-kWh incentive	k_{DR}	0.2—0.35 CNY/kWh
Aggregate line loss in buy–sell process	P_l	6%
Maximum selling power	$P_{s,\max}$	48 MW
Minimum selling power	$P_{s,\min}$	8 MW
Total controllable load power in the park	P_{all}	28 MW

losses in buy-sell transactions are assumed to be 3%. A progressive interruption test is implemented via an IoT sensing network (including smart meters and PLC controllers) to record key parameters such as the maximum interruption duration and response delay; the sampling frequency is set at the second level to capture dynamics. Historical data are extracted from the Demand Response Management System (DRMS) event logs over the past three years. All data acquisition complies with relevant standards, and digital-signature techniques are used to ensure reliable traceability. The simulation's load-monitoring horizon is 24 h, with data exported every 15 min; other variable settings are listed in Table 8.

Additionally, all subsequent scenarios are implemented in MATLAB, and the solution is obtained via an iterative genetic algorithm. The population size is set to 50, the number of generations to 100, and the crossover and mutation probabilities to 80% and 0.05, respectively. The convergence tolerance is $\varepsilon = 1 \times 10^{-6}$.

As shown in Fig. 8, the baseline daily load curves for both residential and non-residential users exhibit a "flat → rise → midday, valley → evening peak → decline" pattern. After introducing the LA, peak-period loads are capped at roughly 70% of the baseline peak, and after 22:00 they recover with a controlled ramp, markedly reducing the peak–valley gap. Non-residential loads respond more intensively within the high-price window of 14:00–21:00. By contrast, residential loads show slightly smaller peak-shaving due to the rigidity of household consumption. This "peak shaving-backfilling" dynamic confirms the soundness of the proposed model in terms of constraint design and response-behavior simulation, and it provides a reliable baseline for subsequent multi-scenario comparisons.

5.2. Scenario design and analysis of operating results

To further validate the model and the game-theoretic conclusions, and to examine how different conditions affect LA pricing, three representative simulation scenarios are designed, as shown in Table 9: (1) a summer high-temperature tariff scenario; (2) a holiday consumption-behavior scenario; and (3) a park with a higher industrial share. Holding other basic parameters constant, comparative simulations are conducted; the resulting LA profits are shown in Fig. 9. Relative

Table 9
Scenario settings for each case.

Scenario description	Differential settings
Baseline	Spring tariff; balanced-type park (industry/commercial-industrial/residential shares: 50%/20%/30%); weekday routine consumption behavior
Summer tariff	Summer tariff; balanced-type park (industry/commercial-industrial/residential shares:50%/20%/30%); weekday routine consumption behavior
Holiday consumption behavior	Spring tariff; balanced-type park (industry/commercial-industrial/residential shares:50%/20%/30%); holiday-specific consumption behavior
VPP park with higher industrial share	Spring tariff; industrial-dominant park (industry/commercial-industrial/residential shares:70%/20%/10%); weekday routine consumption behavior

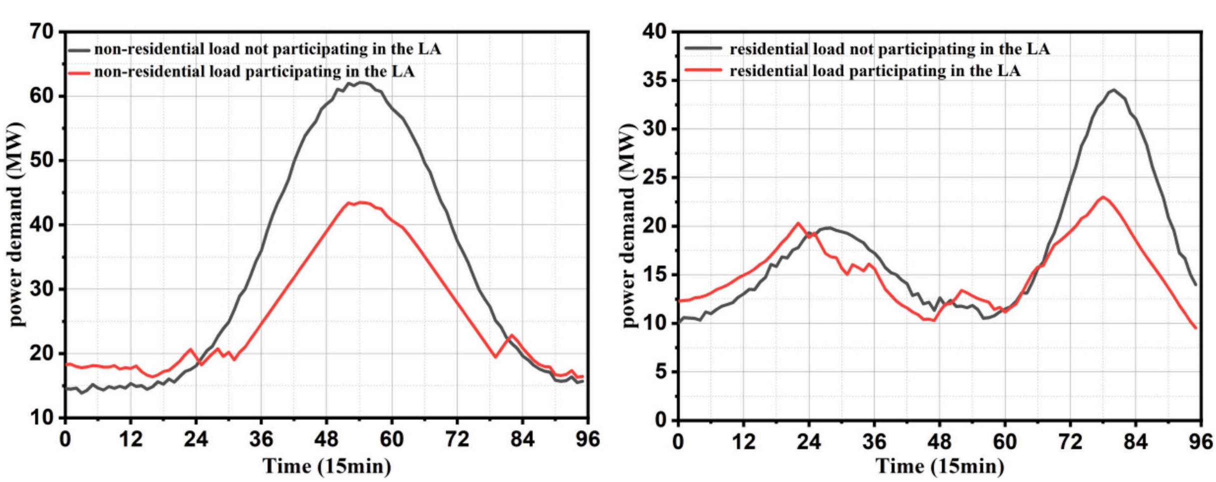

Fig. 8. Comparison of baseline daily load curves.

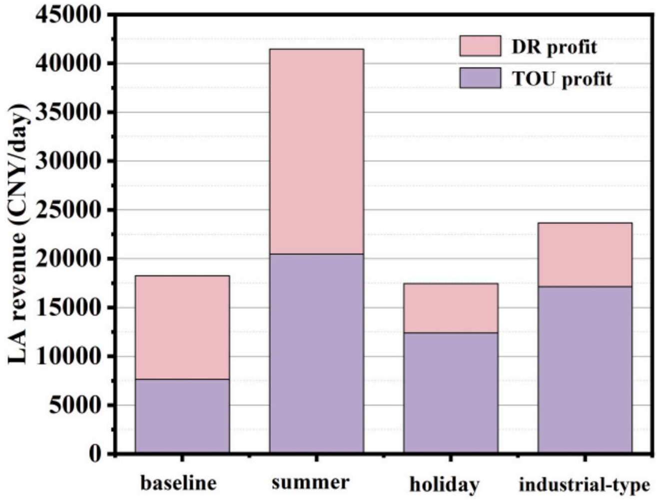

Fig. 9. Comparison of LA revenue sources under different scenarios.

to the baseline, in the summer high-temperature tariff scenario the LA's net profit increases by 108.6%, and the average retail price is 9.8% lower than the external grid price in August. In the holiday scenario, profit decreases by 3.6% and the retail price is 7.1% below the external grid price. In the high-industrial-share scenario, profit rises by 11.9% and the retail price falls by 10.6%.

Fig. 9 also reveals the composition of LA revenues, which mainly derive from two sources: (i) peak-shaving and valley-filling gains enabled by time-of-use pricing, and (ii) DR compensation triggered when the system load factor crosses preset thresholds. In the summer high-temperature scenario, the system load factor remains elevated, so the share of DR compensation rises markedly—reflecting the amplification effect of higher unit compensation at high load factors. During holidays, peak pressure on the system eases; accordingly, the share of peak-shaving/valley-filling gains increases, while the DR-compensation share declines. When the industrial load share increases, the park has greater adjustable capacity during peak periods, so both revenue components rise, though peak-shaving/valley-filling remains the dominant source overall. Taken together, the model stably captures market-signal variations and user-side response characteristics under heterogeneous operating conditions, providing a feasible basis for optimizing differentiated pricing strategies for LAs.

Differentiated responses of residential and non-residential users under the three scenarios are shown in Figs. 10–12. In the summer high-temperature scenario, cooling demand rises in step with the system load factor; the LA induces stronger peak-shaving/valley-filling effects within the 14:00–21:00 window, yielding the largest evening-peak reduction among all scenarios. Under the holiday scenario, both total load and the peak-valley gap decline, and the LA primarily captures price-spread gains during the flat and off-peak periods. In the industrial-park scenario, working hours more readily exhibit a "concentrated rise—rapid

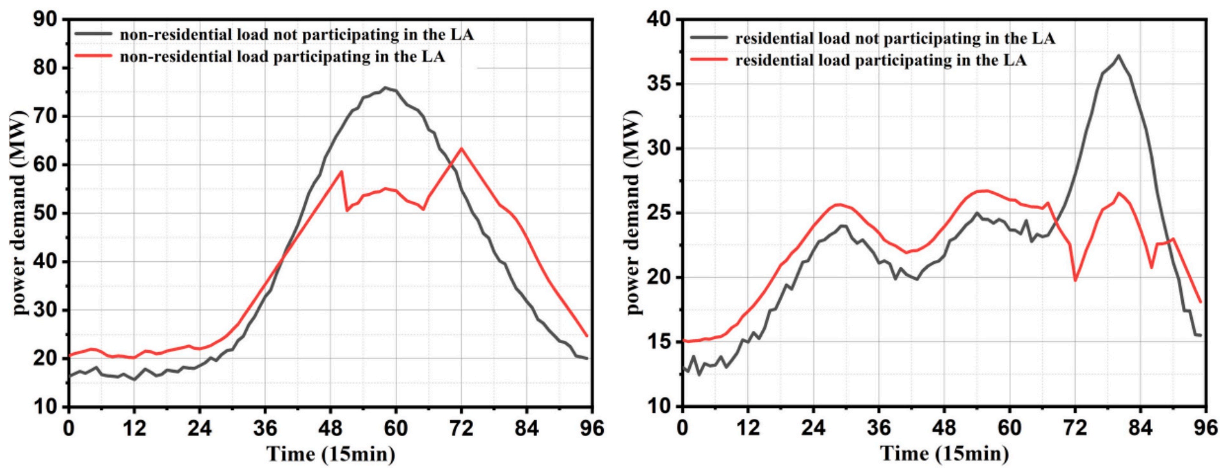

Fig. 10. Daily load curve comparison under summer tariffs.

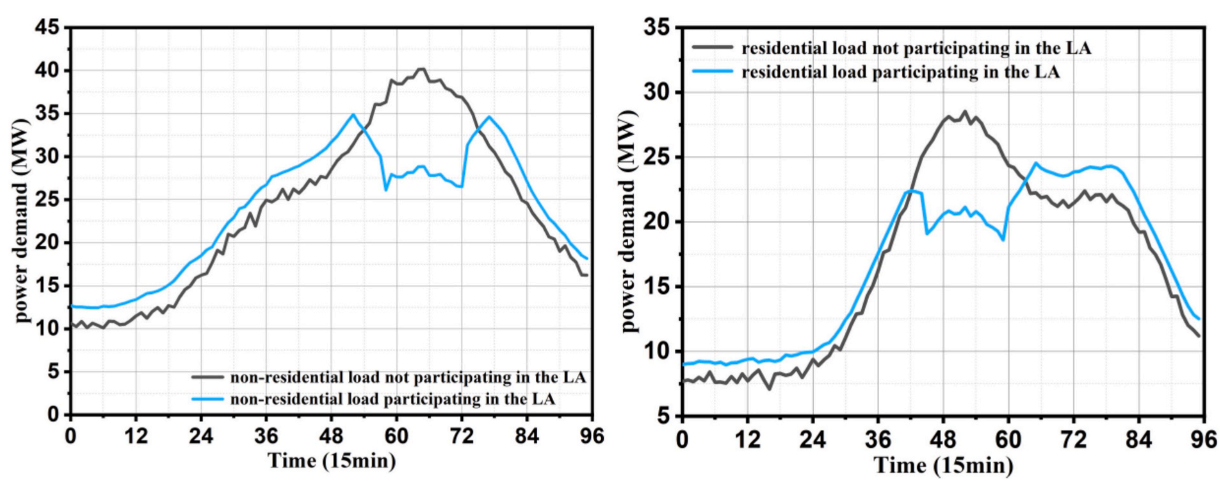

Fig. 11. Holiday daily load curve comparison.

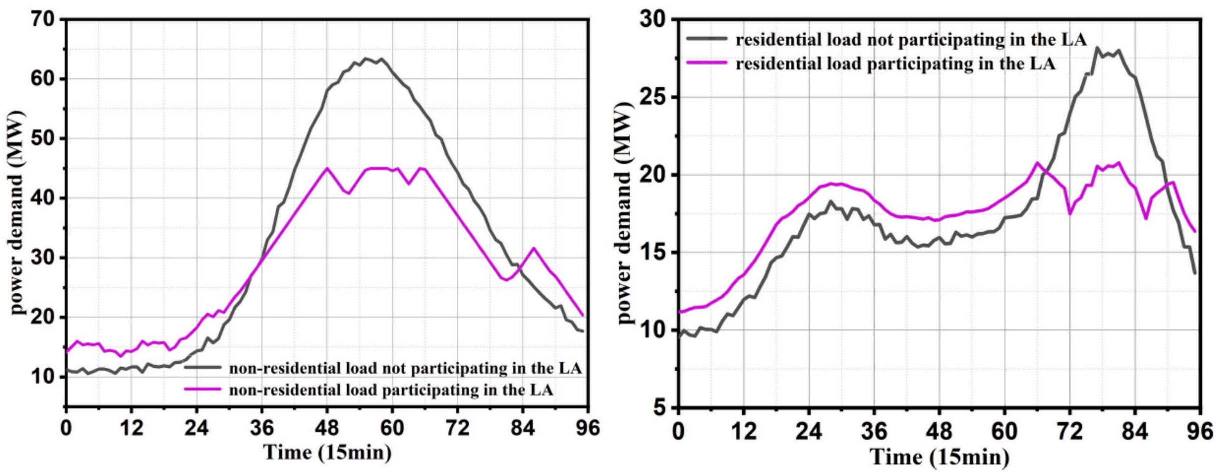

Fig. 12. Daily load curve comparison for an industrial-type park.

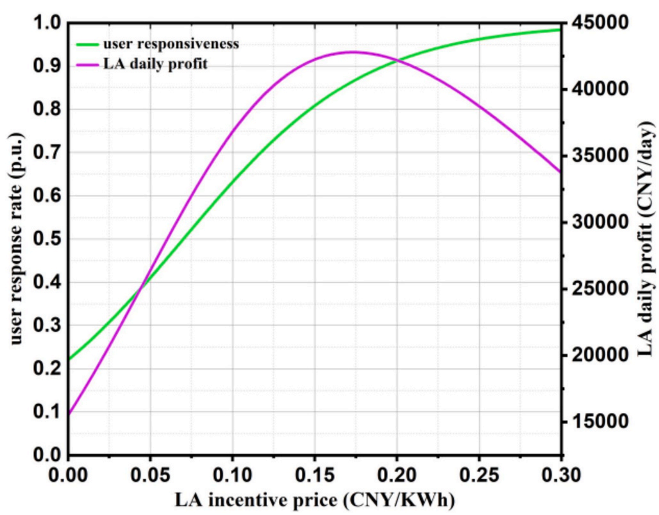

Fig. 13. LA incentive-response and profit curves.

fall" profile; by scheduling shiftable processes and non-critical operations, the LA substantially suppresses peak-period load while avoiding a secondary peak. Together, the three scenarios indicate that price-signal strength and load transferability are the key determinants of LA responsiveness: when price volatility is pronounced and the share of transferable load is high, the LA's load-control potential and market revenues both increase significantly.

It should be noted that LA revenue is not strictly positively correlated with the user response rate. The response rate is directly influenced by the incentive price set by the LA; however, excessively high incentives erode the LA's profit. As shown in Fig. 13, under the baseline setting the LA's average incentive payment is best placed in the range of 0.15–0.20 CNY/kWh to achieve the highest possible revenue.

Overall, the proposed LA pricing model converges stably across scenarios, delivering higher LA profits and lower user electricity-purchase costs. The improvements are more pronounced when the daily peak-valley gap is larger or the industrial share is higher. Moreover, by comparing daily load curves before and after contracting with the LA, the trajectories become noticeably smoother, indicating that the model has strong applicability and practical value for coordinating peak-shaving/valley filling and DR.

6. Conclusion

Focusing on real-time retail pricing for LAs within a VPP context, this study proposes a two-stage "clustering-game pricing" analytical framework. First, K-means++ clustering is performed on features such as historical load, price, and transferability to identify differentiated user clusters and adjustable potential. Building on this, a Stackelberg game is formulated with the LA as leader and end users as followers, wherein retail price, per-kWh compensation, and incentive budgets are jointly optimized to reach equilibrium. Using actual tariffs and load curves, we design scenarios—summer high load "holiday travel" and "higher industrial share"—to evaluate the model's effectiveness and robustness across dimensions of profit, cost, peak–valley gap, and user response. The main contributions are as follows:

(1) The proposed LA real-time pricing model combines multi-dimensional electricity-use clustering with a Stackelberg game, and—through coordinated optimization using a genetic algorithm and exact solvers—significantly enhances the synergy between peak-shaving/valley filling and profit maximization while improving model robustness.
(2) Under the baseline scenario, non-residential and residential users' electricity-purchase costs fall by approximately 3.57% and 2.45%, respectively. Across multiple simulation scenarios, the LA's net profit increases steadily—particularly under summer high-load conditions—and a higher industrial share likewise delivers notable profit gains. Meanwhile, the average retail price is about 7%-10% lower than the external grid price.
(3) Price signals and load transferability jointly drive peak-shaving and valley filling: peak-period loads are effectively suppressed, nighttime replenishment is smooth, and the load curve becomes more uniform. When the peak-valley gap is larger or the share of adjustable loads increases, system peak-regulation benefits and renewable-energy accommodation capacity are further enhanced.
(4) User response rates rise with higher per-kWh incentives, but overly generous incentives erode LA profits. Under the baseline scenario, incentive compensation is best set in the 0.15–0.20 CNY/kWh range to balance revenue and participation, providing quantitative guidance for the design of piecewise compensation and its linkage with retail pricing.

In future work, the model can be extended to multi-agent coordinated pricing, dynamic incentive optimization, and user-side behavioral modeling, thereby supporting LAs in real-time pricing and response management under more complex market conditions and providing decision support for enhancing power-market flexibility and optimizing user participation mechanisms.

Data availability statement

The data that support the findings of this study are available from the corresponding author upon reasonable request.

CRediT authorship contribution statement

Xiaolong Yang: Writing – review & editing, Writing – original draft, Supervision, Methodology, Funding acquisition, Conceptualization. **Mengmeng Zhao:** Writing – review & editing, Methodology, Data curation. **Weiyao Gao:** Software, Methodology, Conceptualization. **Shuai Zhou:** Writing – review & editing, Supervision, Methodology. **Jieping Han:** Supervision, Data curation. **Zeqi Ge:** Investigation, Data curation. **Yuhan Liu:** Software, Data curation.

Declaration of competing interest

The authors declare that they have no known competing financial interests or personal relationships that could have appeared to influence the work reported in this paper.

Acknowledgments

This study was supported by the National Social Science Fund of China (Project No. 24BJY141)

Data availability

Data will be made available on request.

References

[1] Shen Y, Cen W, Zhou B. Optimization strategy for the joint energy and peak-shaving market of virtual power plants considering differentiated bidding of power supply equipment. Electr Power Mark 2025;58(7):115–27. https://doi.org/10.11930/j.issn.1004-9649.202412113.
[2] Cheng Y, Zhang N, Zhang B, Kang C, Xi W, Feng M. Low-carbon operation of multiple energy systems based on energy-carbon integrated prices. IEEE Trans Smart Grid 2020;11(2):1307–18. https://doi.org/10.1109/TSG.2019.2935736.
[3] Kang J, Li Y, Chen Q, Mai D, Hao B, Li Y. Construction and operational exploration of a virtual power plant model based on building load aggregation. Power Supply 2025;42(4):59–68. https://doi.org/10.19421/j.cnki.1006-6357.2025.04.008.
[4] Wang J, Xu J, Wang J, Ke D, Yao L, Zhou Y, et al. Two-stage distributionally robust offering and pricing strategy for a price-maker virtual power plant. Appl Energy 2024;363:123005. https://doi.org/10.1016/j.apenergy.2024.123005.
[5] He H, Ren Z, Gao Y. Power system scheduling method considering the characteristics of a green-hydrogen chemical virtual energy pool. Electr Power Autom Equip 2025;8(25):44–50. https://doi.org/10.16081/j.epae.202508014.
[6] Zhao Z, Xie B. LCOE analysis of wind power systems under multiple penetration levels. Mod Electr Power 2024;41(6):37–49. https://doi.org/10.19725/j.cnki.1007-2322.2022.0367.
[7] Cao J, Yang D, Dehghanian P. Cooperative operation for multiple virtual power plants considering energy-carbon trading: a Nash bargaining model. Energy 2024;307:132813. https://doi.org/10.1016/j.energy.2024.132813.
[8] Sun W, Liu X, Xiang W, Li H. Optimal day-ahead pricing strategy for load aggregators based on a Stackelberg game. Autom Electr Power Syst 2021;45(1):159–67. https://doi.org/10.7500/AEPS20200519003.
[9] Zhang D, Zhu H, Zhang H, Goh HH, Liu H, Wu T. Multi-objective optimization for smart integrated energy system considering demand responses and dynamic prices. IEEE Trans Smart Grid 2022;13(2):1100–12. https://doi.org/10.1109/TSG.2021.3128547.
[10] Wang F, Ge X, Li K, Mi Z. Day-ahead market optimal bidding strategy and quantitative compensation mechanism design for load aggregator engaging demand response. IEEE Trans Ind Appl 2021;55(06):5564–73. https://doi.org/10.1109/TIA.2019.2936183.
[11] Muñoz FD, Wogrin S, Oren SS, Hobbs BF. Economic inefficiencies of cost-based electricity market designs. Energy J 2020;39(3):51–76.
[12] Wei L, Li Y, Xie B, Xu K, Meng G. Two-stage optimal scheduling based on the meteorological prediction of a wind-solar-energy storage system with demand response. Energies 2024;17(06):1286. https://doi.org/10.3390/en17061286.
[13] Sun C, Mu C. Several key scientific issues in multi-agent deep reinforcement learning. Acta Autom Sin 2020;46(7):1301–12. https://doi.org/10.16383/j.aas.c200159.
[14] Ekoue MK, Woerman M, Clastres C. Intermittency and uncertainty in wind and solar energy: Impacts on the French electricity market. Energy Econ 2025;142:108176. https://doi.org/10.1016/j.eneco.2024.108176.
[15] Perera A, Kamalaruban P. Applications of reinforcement learning in energy systems. Renew Sust Energy Rev 2021;137:110618. https://doi.org/10.1016/j.rser.2020.110618.
[16] Pesántez G, Guamán W, Córdova J, Torres M, Benalcazar P. Reinforcement learning for efficient power systems planning: a review of operational and expansion strategies. Energies 2024;17(9):2167. https://doi.org/10.3390/en17092167.
[17] Li M, Wang Y, Zhang Y, Tan Q, Wu P, Wu Y. Mechanism of the impact of time-of-use pricing on load characteristics based on multi-dimensional price elasticity coefficients. Electr Power 2024;57(2):202–11. https://link.cnki.net/urlid/11.3265.TM.20230920.1221.002.
[18] Shan L, Song H, Tang Q, Guo H, Hou S, Kang C. Analysis and insights into power balancing mechanisms under decentralized decision-making: the case of Germany's balancing settlement units. Power Syst Technol 2025;49(4):1436–46. https://doi.org/10.13335/j.1000-3673.pst.2024.1272.
[19] Song Y, Chae M, Chu Y, Yoon Y, Jin Y. Impact of penalty structures on virtual power plants in a day-ahead electricity market. Energies 2024;17(23):6042. https://doi.org/10.3390/en17236042.
[20] Fan W, Fan Y, Yao X, Yi B, Jiang D, Wu L. Distributed transaction optimization model of multi-integrated energy systems based on Nash negotiation. Renew Energy 2024;225:120196. https://doi.org/10.1016/j.renene.2024.120196.
[21] Fang Y, Hu J, Ma W. Stackelberg game-based optimal scheduling strategy for electric vehicle aggregators considering user willingness. Trans China Electrotech Soc 2023;39(16):1436–46. https://doi.org/10.19595/j.cnki.1000-6753.tces.230923.
[22] Wu T, Hui H, Zhang H. A review of commercial building air-conditioning systems participating in urban power grid load regulation. Electr Power 2023;56(7):1–11. https://doi.org/10.11930/j.issn.1004-9649.202209064.
[23] Liu Z, Huang B, Li Y, Sun Q, Pedersen TB, Gao DW. Pricing game and blockchain for electricity data trading in low-carbon smart energy systems. IEEE Trans Ind Inf 2024;20(4):6446–56. https://doi.org/10.1109/TII.2023.3345450.
[24] Afroz Z, Strbac G, Mancarella P. Energy flexibility of commercial buildings for demand response: a bottom-up physics-based characterization approach. Energ Build 2023;300:113533. https://doi.org/10.1016/j.enbuild.2023.113533.
[25] Liu J, Hu H, Yu SS, Trinh H. Virtual power plant with renewable energy sources and energy storage systems for sustainable power grid—formation, control techniques and demand response. Appl Energy 2023;16(09):3705. https://doi.org/10.3390/en16093705.
[26] Sun Q, Yao J, Wang Y. From virtual power plants to actual energy: a review and prospects of VPP research. Power Gener Technol 2023;44(5):584–602. https://doi.org/10.12096/j.2096-4528.pgt.23102.
[27] Zhang T, Wang L, Sun Y, Yu A, Zheng K, Guo H, et al. Pricing strategy for shared energy storage and day-ahead optimal decisions of park users based on a Stackelberg game. Demand Side Manage Electr Power 2023;25(4):1–7. https://doi.org/10.3969/j.issn.1009-1831.2023.04.001.
[28] Zheng Q, Yang P, Wu Y, Xu Z, Zhang P. Aggregation dispatch and control strategies for multi-type loads in industrial parks. Appl Sci 2023;13(16):9205. https://doi.org/10.3390/app13169205.
[29] Zhou R, Zhao Y, Hu F, Huang C. Green power market-carbon market coupled trading based on improved electricity carbon accounting. Proc CSU-EPSA 2024;36(2):105–15. https://doi.org/10.19635/j.cnki.csu-epsa.001282.
[30] Zou M, Wang W, Liu M, Jia H, Su S, Yang Y, et al. Value assessment of electric vehicle aggregation operation based on a value network. Mod Electr Power 2023;40(12):45–52. https://doi.org/10.19725/j.cnki.1007-2322.2022.0130.
[31] Lu X, Qiu J, Zhang C, Lei G, Zhu J. Seizing unconventional arbitrage opportunities in virtual power plants: a profitable and flexible recruitment approach. Appl Energy 2024;358:122628. https://doi.org/10.1016/j.apenergy.2024.122628.
[32] Ning B, Han Q-L, Zuo Z, Ding L. Accelerated secondary frequency regulation and active power sharing for islanded microgrids with external disturbances: a fully distributed approach. Automatica 2025;174:112146. https://doi.org/10.1016/j.automatica.2025.112146.
[33] Maiz S, Baringo L, García-Bertrand R. Dynamic expansion planning of a commercial virtual power plant through coalition with distributed energy resources considering rival competitors. Appl Energy 2025;377:124665. https://doi.org/10.1016/j.apenergy.2024.124665.
[34] Sun Y, Jiang Y, Lv J. Bidding optimization of aggregators considering safety check in a distribution network. Electr Eng 2023;105(6):3813–24. https://doi.org/10.1007/s00202-023-01884-6.
[35] Dahiwale PV, Rather ZH, Mitra I. A comprehensive review of smart charging strategies for electric vehicles and way forward. IEEE Trans Intell Transp Syst 2024;25(9):10462–72. https://doi.org/10.1109/TITS.2024.3365581.
[36] Miraftabzadeh SM, Colombo CG, Longo M, Foiadelli F. K-means and alternative clustering methods in modern power systems. IEEE Access 2023;11:119596–633. https://doi.org/10.1109/ACCESS.2023.3327640.
[37] Mukherjee S, Vuillon L, Dutykh D, Tsanakas I. Scalable weather data reduction for solar PV analysis using graph-based approach. Energy Syst 2025:1–26. https://doi.org/10.1007/s12667-025-00767-y.
[38] Huang C, Li K, Zhang N. Strategic joint bidding and pricing of load aggregators in day-ahead demand response market. Appl Energy 2025;377:124552. https://doi.org/10.1016/j.apenergy.2024.124552.

[39] Üstündağlı Erten E, Janghorban Esfahani I, Ifaei P, Güzeloğlu EB. Dwelling, habits, and possessions: Clustering Turkey's household energy choices through responsible consumption and poverty. Energies 2023;16(24):7983. https://doi.org/10.3390/en16247983.

[40] Chen Y-H, Li Y-Z, Jiang H, Huang Z. Research on household energy demand patterns, data acquisition and influencing factors: a review. Sust Cities Soc 2023;99:104916. https://doi.org/10.1016/j.scs.2023.104916.

[41] Ridzuan F, Zainon WMN. A review on data cleansing methods for big data. Proc Comput Sci 2019;161:731–8. https://doi.org/10.1016/j.procs.2019.11.177.

[42] Zhang K, Liu S, An S, Zhou Y, Pu X. Towards high-efficiency self-powered wireless sensor networks: a systematic review of co-design of energy and signal. Nano Energy 2025;144:111337. https://doi.org/10.1016/j.nanoen.2025.111337.

[43] Ren Z, Li S, Guo J, Lin D, Dong Y. A bi-level optimization framework for virtual power plants integrating electric vehicles and demand response. Sust Energy Technol Assess 2025;84:104740. https://doi.org/10.1016/j.seta.2025.104740.

[44] Luan W, Tian L, Zhao B. Leveraging hybrid probabilistic multi-objective evolutionary algorithm for dynamic tariff design. Appl Energy 2023;342:121123. https://doi.org/10.1016/j.apenergy.2023.121123.